Magnetic Resonance in Medicine 62:1394–1403 (2009)

Quantification of Non–Water-Suppressed MR Spectra With Correction for Motion-Induced Signal Reduction

Jyh-Miin Lin,[1] Shang-Yueh Tsai,[2*] Hua-Shan Liu,[1,3] Hsiao-Wen Chung,[1] Robert V. Mulkern,[4,5] Chou-Min Cheng,[6] Tzu-Chen Yeh,[6] and Nan-Kuei Chen[7]

Intrascan subject movement in clinical MR spectroscopic examinations may result in inconsistent water suppression that distorts the metabolite signals, frame-to-frame variations in spectral phase and frequency, and consequent reductions in the signal-to-noise ratio due to destructive averaging. Frame-to-frame phase/frequency corrections, although reported to be successful in achieving constructive averaging, rely on consistent water suppression, which may be difficult in the presence of intrascan motion. In this study, motion correction using non–water-suppressed data acquisition is proposed to overcome the above difficulties. The time-domain matrix-pencil postprocessing method was used to extract water signals from the non–water-suppressed spectroscopic data, followed by phase and frequency corrections of the metabolite signals based on information obtained from the water signals. From in vivo experiments on seven healthy subjects at 3.0 T, quantification of metabolites using the unsuppressed water signal as a reference showed improved correlation with water-suppressed data acquired in the absence of motion (R^2 = 0.9669; slope = 0.94). The metabolite concentrations derived using the proposed approach were in good agreement with literature values. Computer simulations under various degrees of frequency and phase variations further demonstrated robust performance of the time-domain postprocessing approach. Magn Reson Med 62:1394–1403, 2009. © 2009 Wiley-Liss, Inc.

Key words: non–water suppressed MRS; in vivo single voxel spectroscopy; motion correction; spectral processing; signal restoration

Inevitable subject motions during successive data acquisition in magnetic resonance spectroscopy (MRS) may cause signal loss because of two major mechanisms (1-4). First, motion-induced magnetic field drifts may lead to frequency shift over multiple MRS acquisition frames. Second, subject movements in the presence of the spoiler gradients may result in inconsistent phase variations among acquisition frames. In conventional MRS studies, data from all acquisition frames are simply averaged, and therefore the destructively averaged spectrum would be affected by signal-to-noise ratio (SNR) attenuation and spectral shape distortion because of frame-to-frame phase/frequency variations. It has been shown that, by performing frame-by-frame corrections for the intrascan phase/frequency variations, the constructively averaged MRS data exhibit significantly improved SNR and spectral quality (1-8). The search for an effective intrascan phase/frequency correction method is thus an active field of research for in vivo MRS.

Over the past decades, several methods have been proposed to measure the intrascan phase/frequency variations in MRS scans in order to perform constructive averaging (1,2,4-6). In one of these methods, the non–water-suppressed (NWS) free induction decay and water-suppressed (WS) MRS data were acquired in an interleaved manner (2). Intrascan phase/frequency variations estimated from the NWS free induction decay were used to correct the WS MRS data. In this approach, however, the phase variations in WS MRS data are corrected by values estimated at different time points. Therefore, the effectiveness of the phase correction might be suboptimal, particularly in the presence of abrupt intrascan movements.

Alternatively, the phase variations induced by intrascan motion could be measured on a frame-by-frame basis directly from the residual water signals of WS MRS data (1,4). However, even though the information estimated directly from the WS MRS data better reflects the instant phase variation in comparison to the interleaved free induction decay-based measurements, this approach has two main limitations: First, the residual water signals in WS MRS data have low SNR that limits the accuracy of frame-by-frame phase estimation (1). Second, the residual water signals strongly depend on the efficiency of water suppression pulses and may be easily distorted in brain regions affected by pronounced field inhomogeneities, particularly when the water suppression efficiency varies due to intrascan subject movement (2). The intrascan subject movement not only results in MRS line-shape distortion and SNR reduction but also makes it difficult to perform absolute metabolite quantification. The calibration spectra (i.e., the reference for MRS quantification) acquired before the actual MRS scan may become invalid due to changes of the subject position (1).

It has been shown recently that the water signals may be removed in postprocessing even when no water-suppression pulse is applied during MRS data acquisition. The NWS MRS is potentially superior to WS MRS in several ways (9-12). First, the metabolite signals in NWS MRS are not distorted by the water suppression pulses (13). Sec-

[1]Department of Electrical Engineering, National Taiwan University, Taipei, Taiwan

[2]Department of Electrical Engineering, Chang-Gung University, Tao-Yuan, Taiwan

[3]Department of Radiology, Tri-Services General Hospital and National Defense Medical Center, Taipei, Taiwan

[4]Department of Radiology, Brigham and Women's Hospital, Harvard Medical School, Boston, MA, USA

[5]Department of Radiology, Children's Hospital, Harvard Medical School, Boston, MA, USA

[6]Department of Radiology, Taipei Veterans General Hospital, Taipei, Taiwan

[7]Brain Imaging and Analysis Center, Duke University, Durham, NC, USA

*Correspondence to: Shang-Yueh Tsai, PhD, Assistant Professor, Department of Electrical Engineering, Chang-Gung University, No. 245, Wen-Hua 1st Road, Kwei-Shan, Tao-Yuan, Taiwan, 333. E-mail: syytsai@gmail.com

Received 19 November 2008; revised 12 May 2009; accepted 28 May 2009.
DOI 10.1002/mrm.22119
Published online 24 September 2009 in Wiley InterScience (www.interscience.wiley.com).

ond, the unsuppressed water signals can be used as an internal reference for absolute metabolite quantification (12). Here in this study we further show that, with appropriate postprocessing methods to separate the water signals from the metabolite signals, the NWS MRS technique enables a reliable frame-by-frame correction of intrascan motion-related artifacts using information derived from the high-SNR unsuppressed water signals. Single voxel spectroscopy experiments were performed to demonstrate the effectiveness of the proposed method.

THEORY

Signal Loss Due to Frequency/Phase Variations in Sequential Scans

The use of unsuppressed water signals in NWS spectra to correct for motion-related signal loss is based on the assumption that the time signals obtained in the same voxel experience similar frequency/phase shifts for water and the metabolites. Therefore, the time-domain MR signals sampled at the nth point, $S(n)$, can be explicitly written as the summations of all the metabolites M and the water:

$$S(n) = A_{H2O}e^{i(\phi H20+\Delta\phi)}e^{[-\alpha H20+i2\pi(fH20+\Delta f)]\tau-n} + \sum_{M} A_M e^{i(\phi m+\Delta\phi)}e^{[-\alpha m+i2\pi(fM+\Delta f)]\tau\cdot n} \quad [1]$$

where A_{H2O} and $A_{metabolite}$ are the signal amplitudes of water and metabolites, respectively, which are related to spin density, relaxation parameters T_2 and T_1, as well as acquisition parameters echo time and pulse repetition time. ϕ_{H2O} and $\phi_{metabolite}$ are the initial phases, and $\Delta\phi$ is the relative phase shift due to intrascan motion. α_{H2O} and $\alpha_{metabolite}$ are the rate constants as a function of relaxation parameters T_2*. f_{H2O} and $f_{metabolite}$ are the resonant frequencies, and Δf is the relative frequency shift due to intrascan motion. τ stands for the data sampling interval.

Restoration of Phase and Frequency Shifts for Constructive Averaging

The signal loss and line-broadening effects can be reversed by scan-to-scan correction, also named "constructive averaging" (1). For a successful constructive averaging, the first step is to measure the phase shift $\Delta\phi$ and frequency shift Δf for each MRS scan. The second step is to reverse the phase/frequency variation in each scan. Finally, the corrected spectra are averaged to get a constructively averaged spectrum. The only limitation of the constructive averaging lies in how close one can measure the actual phase and frequency variations. It is for this reason that NWS acquisition is preferred over WS acquisition, due to improved estimations in the presence of high SNR such that the residual errors in phase (ε_ϕ) and in frequency (ε_f) are minimized.

Estimation of Phase and Frequency Shift in the Frequency Domain

Intuitively, estimation of phase and frequency variation can be accomplished in the frequency domain. The N-point discrete Fourier transform of the free induction decay signals is:

$$X(k) = \sum_{n=0}^{N-1}[A_{H_2o}e^{(\phi H2O+\Delta\phi)}e^{[-\alpha_{H2o}+i2\pi(f_{H20}+\Delta f)]\tau-n} + \Sigma_M A_M e^{i(\phi_M+\Delta\phi)}e^{[-\alpha_M+i2\pi(f_M+\Delta f)]\tau\cdot n}e^{\frac{2m}{N}nk} \quad [2]$$

For phase estimation, only the water signal is considered. Therefore, the estimation of Δf is based on the shift of reference water peak that satisfies $(-\frac{k}{N\cdot\tau + f_{H2O} + \Delta\cdot f) = 0}$ and leading to $k = N\cdot\tau\cdot(f_{H2O} + \Delta f + \varepsilon_f)$. One notices, however, that the residual frequency error is given by $\varepsilon \geq \frac{1}{N\tau}$. The phase is estimated at the water peak. The signal at $k = N\cdot\tau\cdot(f_{H2O} + \Delta f + \varepsilon_f$ is $A_{H2O}e^{i(\phi_{H2O}+\Delta\phi)} \times \left(\frac{1-e^{[-\alpha_{H2o}+i2\pi\varepsilon_f]\tau\cdot N}}{1-e^{[-\alpha_{H2O}+i2\pi\varepsilon_f]\tau}}\right)$, which essentially indicates that there is a lower limit of the phase error given by

$$\varepsilon_\phi \geq \angle\left(\frac{1-e[-\alpha_{H2O}+i2\pi\varepsilon_f]\tau\cdot N}{1-e[-\alpha_{H2O}+i2\pi\varepsilon_f]\tau}\right) \quad [3]$$

It is evident that if Δf can be accurately measured, a reduction in phase error is possible.

Estimation of Phase and Frequency Shift in the Time Domain

The time-domain methods are basically similar to the frequency-domain methods, for which the mutual difference should be minor at the same SNR level. Previous reports have shown that frequency-domain or time-domain parametric modeling can achieve consistent quantification for metabolites (14,15). Therefore, we expect that both frequency-domain and time-domain methods can benefit from NWS MRS because of the high SNR of water signal. The main advantage of time-domain over frequency-domain approaches is that the time-domain methods have been proven to be able to successfully extract the unsuppressed water signals from NWS spectra for further processing (11,12); thus, the phase and frequency shift can be directly estimated from the extracted water peak. In addition, the mathematical model function in the time domain is easy to compute by some efficient algebraic approaches (16). It can also be easily adapted for the changes in signals due to such factors as imperfect shimming and corruption of the first several points, or due to fast decaying signals (17). In practice, several time-domain algorithms have been proposed to estimate the phase and frequency of water signal. In this study, we have chosen the matrix-pencil method (MPM) for such a purpose. In short, the MR signals are first constructed to form two Toeplitz matrices, with the noise filtered out using proper singular value decomposition techniques before the generalized Eigen problems are solved. Results from a previous study suggested that MPM shows lower variance and biases compared with linear prediction (18). Thus, the MPM approach seems to be suitable for fitting the unsuppressed

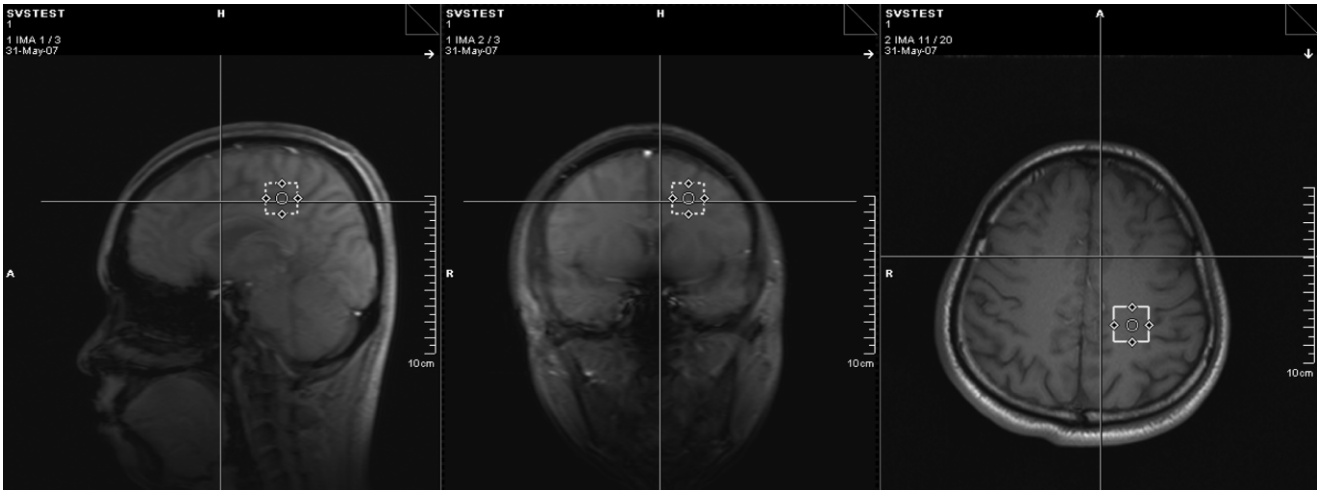

FIG. 1. Spatial location of 20 × 20 × 20 mm^3 volume of interest (box) in the single-voxel spectroscopy experiments.

water signals. Truncated singular value decomposition was used to evaluate the most prominent Eigen value from the matrix-pencil structure constructed from the time-domain data. The most prominent Eigen value represents the water frequency and damping rate, namely, $e[-\alpha_{H2O} + i2\pi\Delta_f]\tau$ in Eq. [1]. The complex amplitude $A_{H_2O}e^{i(\phi_{H2O}+\Delta\phi)}$ is then obtained by least square fitting to derive $\Delta\phi$. For a high-SNR and exponentially decaying reference signal, the biases of phase/frequency estimators have been shown to be both near zero (18). As a consequence, this time-domain approach not only evaluates the phase shift $\Delta\phi$ but also estimates the frequency shift, even if Δf is less than the spectral resolution.

MATERIALS AND METHODS

Simulation

Simulation was performed to validate the phase/frequency correction algorithm. A high-resolution MR spectrum (line width about 3 Hz) was acquired from a phantom with well-controlled water suppression on a 3-T MR system (Trio; Siemens Medical Solutions, Erlangen, Germany). The phantom contained a mixture of metabolite solutions, including choline (Cho), creatine, N-acetylaspartate (NAA), myoinositol, glutamate, and glutamine at appropriate concentrations simulating the human brain conditions. The high-quality spectrum was used as the true spectrum. The simulated NWS MR spectra were then generated by adding exponentially decaying water signals in the time domain, modulated with/without 10-Hz gaussian line-shape broadening, with frequency at 0 Hz (i.e., frequency reference to water) to simulate the unsuppressed water signal. The amplitude of the water signals was subsequently varied to mimic the residual water signal in WS spectra where the water suppression pulse may exhibit varying efficiency. To further simulate motion effects in MRS scans, the gaussian random phase/frequency shifts ($\Delta\phi$ and Δf) with zero mean and different standard deviations (σ_ϕ and σ_f) plus complex gaussian noise were added into the true spectrum. σ_ϕ was set at 1.0

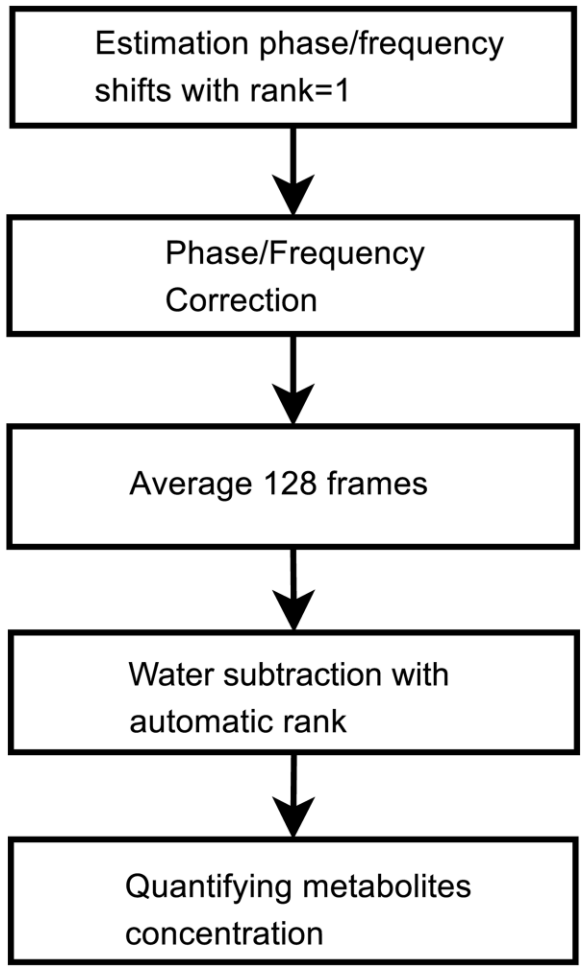

FIG. 2. Flow chart of spectral processing in this study. One especially notices the two-step procedure for water extraction: first using rank = 1 for phase and frequency corrections, and second with automatic rank setting for water signal subtraction, taking into account the line-shape variations under in vivo situations.

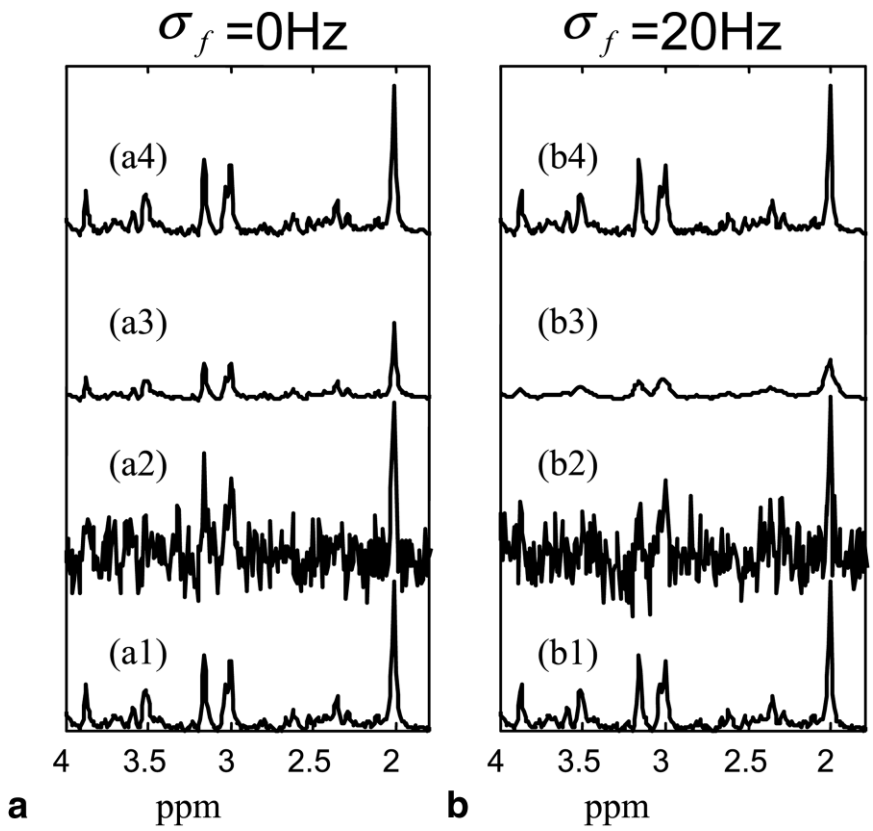

FIG. 3. Comparison of time-domain correction results for 1-rad phase variations between **(a)** no frequency shifts and **(b)** 20-Hz frequency variations. **a1,b1:** Acquired from a phantom with high SNR; regarded as the true spectra. **a2,b2:** The spectra with added noise. The averaged spectra from 128 sets of simulated data are shown in **(a3)** and **(b3)** without correction, and in **(a4)** and **(b4)** after correction using the time-domain method, respectively. Without performing correction, the destructively averaged spectra lead to lowered NAA areas of 67.9% **(a3)** and 50.8% **(b3)** compared with the true spectra. **a4,b4:** The time-domain method restores the NAA area to 94.6% of the true value.

radian, whereas σ_f was varied up to 20 Hz. A total of 128 simulated spectra were averaged to examine the effects of possible destructive averaging. Note that since the purpose of this simulation was to investigate the water signal amplitude effects on the MPM performance, possible lineshape asymmetry in the presence of poor shimming was not included.

Corrections were performed on the simulated spectra before averaging using the time-domain approach. The MPM algorithm was used to fit the first 64 points, with rank set to 1 (18). Then the phase/frequency shifts were reversed. The water components in the corrected NWS spectra were extracted using a singular value decomposition–based algorithm (9). The results in phase errors were compared against the true spectrum. In addition to visual comparison against the true spectrum, the phase errors $|\varepsilon_\phi|$ under different amplitudes of the reference water signal, as well as under different frequency variations, were examined quantitatively.

Subjects and Data Acquisition

For the in vivo experiments, seven healthy volunteers without any histories in psychiatric or neurologic disorders were enrolled in this study under informed consents. All experiments were performed on the same 3-T MR system with an eight-channel coil array that covered the whole brain circumferentially with eight surface receive-only coil elements. An interleaved NWS and WS point-resolved spectroscopy sequence was used to compare the performance of motion correction between the NWS-MRS and the WS-MRS, such that the motion restoration abilities of NWS and WS scans can be compared under similar motion conditions. MRS data were acquired from a selected volume ($2 \times 2 \times 2$ cm^3) located within the parietal lobe, consisting of mostly white matter (Fig. 1), with scan parameters echo time = 40 ms, pulse repetition time = 2 sec, spectral bandwidth = 2 kHz, number of sampling points = 2048. The subjects were instructed to hold their heads still during the "static scan" and to move their heads slightly and randomly during the "motion scan" to evaluate the MRS quality without and with motion, respectively. For the "motion scan," subjects were asked to move the head randomly with arbitrary frequency, which could be as high as 2 Hz and as low as nearly 0 Hz. Subjects were loosely fixed by the two bars close to each side of the ear as the usual configuration of the head coil. Therefore movement was restricted to around 1 cm. During the static sessions, 128 WS scans were acquired and eight NWS scan were acquired using the single-voxel spectroscopy–point-resolved spectroscopy sequences. During the motion sessions, 256 scans using an interleaved NWS and WS point-resolved spectroscopy sequence were acquired and stored separately without signal averaging before postprocessing corrections, hence yielding 128 signal averages for both NWS MRS and WS MRS, respectively. As a result, three data sets were acquired from each subject: (a) WS spectra without motion (static-WS), (b) NWS spectra with motion

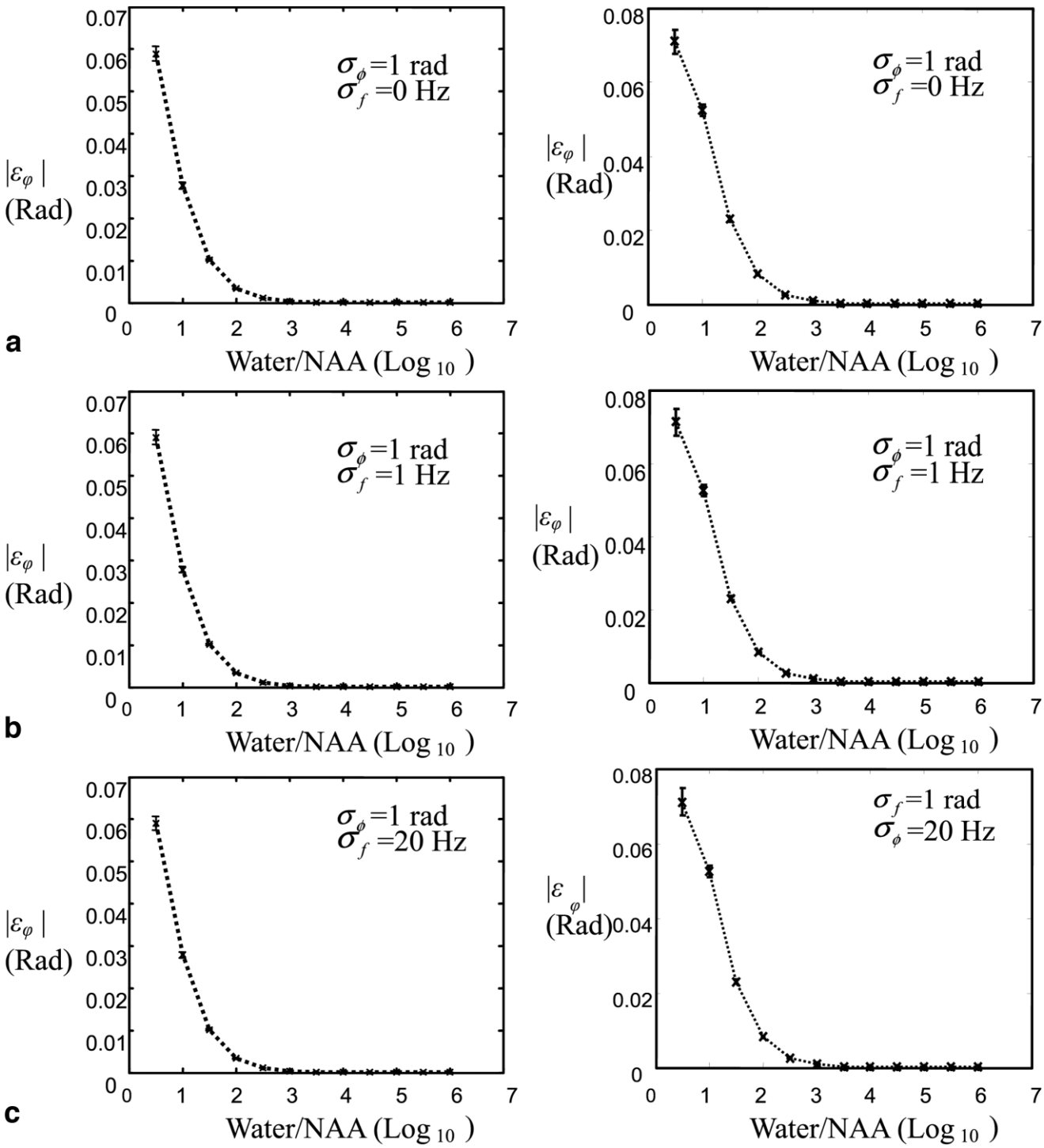

FIG. 4. Simulation results comparing the effectiveness of time-domain corrections at 0 Hz **(a)**, 1 Hz **(b)**, and 20 Hz **(c)** of frequency variations, respectively, plotted for the residual phase errors as a function of water signal intensity (expressed in multiples of the NAA amplitude). Left and right columns represent two different conditions: in the left, the water lines hape is purely Lorentzian, while in the right, the water is convolved with a symmetric gaussian line shape. Note that the advantage of NWS acquisition can be seen in that the time-domain correction method achieves accurate phase corrections when the water signal is larger than 1000-fold of NAA.

(motion-NWS), and (c) WS spectra with motion (motion-WS).

Postprocessing and Quantification

The in vivo spectra were again processed using the time-domain method. Signals from the eight coil elements were averaged with proper phasing in the time domain before corrections (19). The first 128 points of time-domain signal were processed using the MPM algorithm, with rank set to 1 to extract the water signal. Note that for the sole purpose of phase and frequency estimations, setting the rank to 1 was sufficient even if the water spectral line may be asym-

metric in the presence of poor shimming. The phase and frequency shifts estimated from the water signal were then used for motion correction for motion-NWS according to the initial phases of the unsuppressed signals (19). For motion-WS where the water signals were substantially attenuated, motion correction was carried out based on the residual water signal phases estimated from the same time-domain method.

After motion correction, the water signal extracted again using MPM but with rank automatically determined by the theoretical information criteria (18) was subtracted, leaving only the metabolite signals for spectral analysis (9). The reason for using a larger rank setting for water subtraction is that the line shape for water is often asymmetric for in vivo situations. In addition to qualitative comparison on the full width at half maximum of the line width before and after motion correction, the in vivo spectra were quantified with MPM spectral fitting, the range of which was set to 1.8 to 3.3 ppm. Metabolite concentrations of NAA, total creatine (tCr) including creatine and phosphocreatine, and Cho-containing compounds were obtained using the water-scaling method (20). Since our volumes of interest were mostly located in the white matter, the water concentrations were set as 39.2 M (13). The metabolite concentrations shown here were relative values that were not corrected for partial volume effect or T_1, T_2 relaxation. For water scaling in motion-NWS, we used the water signal extracted from the corrected NWS spectra. For static-WS and motion-WS, the water signal of the NWS spectra acquired during the static session was used as the reference. The complete flow chart of spectral processing is shown in Fig. 2.

Statistical Analysis

To evaluate the effectiveness of motion correction on motion-WS and motion-NWS, the concentrations of NAA, tCr, and Cho were compared to those from the static-WS using paired Student's *t* tests.

RESULTS

Simulation Results

The comparison using the time-domain method between two frequency distributions $\sigma_f = 0$ and 20 Hz is shown in Fig. 3a and b, respectively. The phase shift was set to be $\sigma_\phi = 1.0$ radian in both cases. Without frequency shifts, the time-domain method (Fig. 3a4) was effective in the restoration of the NAA area between 1.95 ppm and 2.05 ppm to nearly 94.60%. Even with 20-Hz frequency variations, the time-domain method was still able to successfully restore the NAA peak area to 94.56% of the true spectrum with good preservation of the line width (Fig. 3b4).

With water suppression used during acquisition, the level of reference signals becomes reduced, which might result in difficulties in finding the correct phase/frequency shifts. The effect of reference signal amplitude is shown in Fig. 4, with the amplitude of the reference signal ranging from 10^1 to 10^6 times the NAA. In cases without (Fig. 4; left) and with (Fig. 4; right) gaussian line-shape modulation, the phase errors of the time-domain method were found to markedly increase when reference signal has an amplitude decreasing to levels less than 1000 times NAA, justifying the preferable use of NWS spectra where the water signal is on the order of 10,000 times larger than NAA. With frequency variations $\sigma_f = 1.0$ and 20 Hz, the phase estimation error ε_ϕ using the time-domain method showed similar phase errors as the results without frequency variation. The phase errors were slightly larger in the presence of gaussian broadening.

Table 1
Phase and Frequency Variations of the Seven Subjects

	Motion		Static	
	σ_ϕ (Rad)	σ_f (Hz)	σ_ϕ (Rad)	σ_f (Hz)
Subject 1	1.6922	1.5604	N/A[a]	N/A[a]
Subject 2	1.3282	1.0999	0.0781	0.5203
Subject 3	1.4536	2.4485	0.0588	0.8045
Subject 4	0.5437	2.2028	0.1055	0.6918
Subject 5	0.9549	1.4137	0.0761	0.6336
Subject 6	1.2083	1.6576	0.0435	0.6225
Subject 7	1.0051	1.3262	0.0386	0.8331
Range	0.54∼1.69	1.10∼2.45	0.04∼0.11	0.52∼0.83

[a]The phase/frequency variations for subject 1 were not available because only the averaged spectrum was obtained.

Effectiveness of Motion Correction Using NWS Scans

For the seven volunteers, the motion-induced phase and frequency variations were around ε_ϕ = 0.54 to 1.69 rad (31 ∼ 97°) and σ_f 1.10 to 2.44 Hz, respectively (Table 1). Figure 5 shows the phase and frequency shifts estimated during successive interleaved NWS MRS and WS MRS scans for one subject. It is seen that, even with σ_f around 2 Hz, a non-negligible portion of the data showed frequency variations as large as +3 to –20 Hz. The performance of MPM to extract in vivo water signal in the presence of motion is shown in Fig. 6. The water signal extracted by MPM with rank set to 1 (solid lines) was visually very close to the unsuppressed water (stars). In addition, even if the original in vivo water spectral lines exhibited various degrees of perceivable line-shape asymmetry or broadening, phase and frequency corrections using MPM were still successful. The resulting spectra before and after time-domain motion correction are shown in Fig. 7. Qualitatively, the spectra before motion correction showed broader and partially overlapped metabolite peaks, which may lead to errors in the quantification. The NWS spectral lines restored after motion correction exhibit narrower line width (full width at half maximum ∼10 Hz) than the WS spectral lines (full width at half maximum ∼15 Hz). As a side note, some NWS sidebands arising from gradient coil oscillations (10,21) were visible in the spectra (arrows in Fig. 7). In our study, they were removed by adding/subtracting with spectral data downfield to the water peak, making use of the symmetric property of the gradient oscillation artifacts (10,21).

Fig. 8 shows the metabolite concentrations of NAA, tCr, and Cho as quantified using the time-domain MPM method. Compared with the static-WS scan treated as the true values, the motion-NWS spectra after time-domain motion correction show a statistically insignificant difference ($P > 0.5$), whereas the motion-WS scans exhibit significant reduction in the metabolite concentrations ($P < 0.02$). Correlation analysis shows much better consistency between motion-NWS

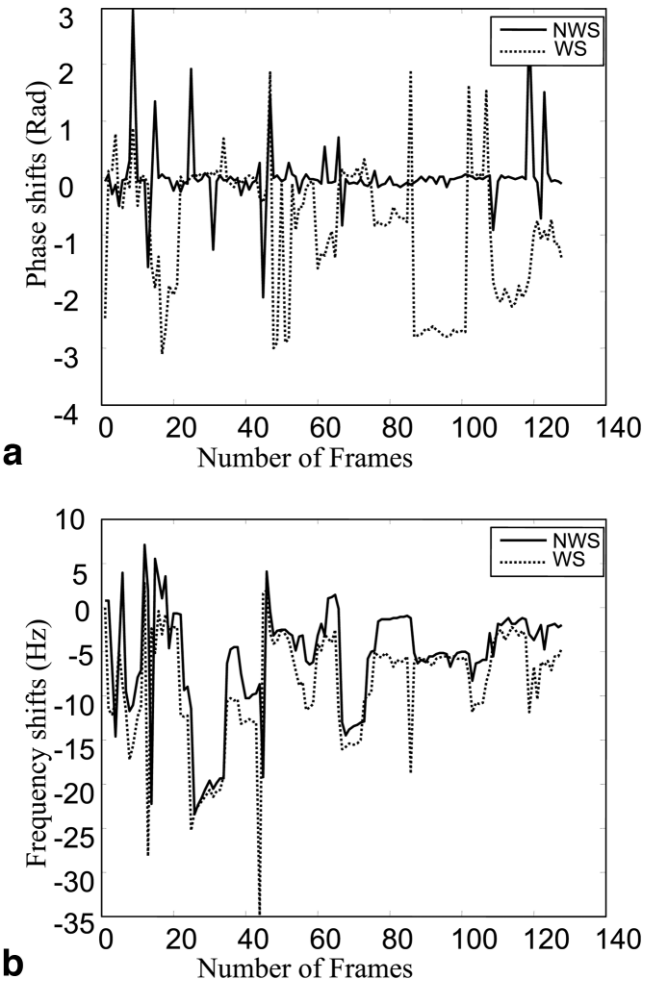

FIG. 5. Representative phase **(a)** and frequency shifts **(b)** due to intrascan movement, estimated from interleaved NWS and WS scans acquired from a subject. During the scan, frequency variations as large as +3 to –20 Hz could be found. Also, the estimated phase and frequency shifts estimated from NWS and WS are somewhat different, likely due to inconsistent water suppression.

and static-WS results (R^2 = 0.9669; slope = 0.94) than between motion-WS and static-WS data (R^2 = 0.7393; slope = 0.69) (Fig. 9). The means and standard deviations of the concentrations for NAA, tCr, and Cho in the white matter as calculated from NWS-motion scans are 13.68 ± 1.83 units, 7.75 ± 1.01 units, and 1.92 ± 0.37 units, respectively, which are in good agreement with values reported in the literature (NAA = 14.26 ± 1.38 mM, tCr = 7.10 ± 0.67 mM, Cho = 2.65 ± 0.25 mM) (13).

DISCUSSION

We have demonstrated the effectiveness of our proposed method to recover motion-induced signal loss on the NWS MRS. Following frame-by-frame corrections for the phase and frequency variations, the constructively averaged data allow accurate quantification of the metabolite concentrations. By using NWS acquisition, problems related to nonideal water suppression, such as incomplete suppression due to field inhomogeneity (2), partial suppression of metabolites (9,12), and differences in coil sensitivity (19,22), are all avoided. Our proposed method is superior to previously reported intrascan MRS motion correction methods in three ways. First, the phase variations are measured from the unsuppressed water signals with high SNR and hence could be estimated more accurately in comparison to estimations based on interleaved NWS scans (2). Second, the metabolite signals are not prone to distortions by the water suppression pulses, which may be inconsistent among frames in the presence of intrascan subject movement (1). Third, the unsuppressed water signal can be used as an internal reference for absolute metabolite quantification (13).

One advantage of our method is that all the procedures are done after data acquisition, hence permitting offline processing without the need to alter data acquisition. The algorithm is computationally economic, with the total processing time being around 2.5 sec on a standard personal computer for one spectrum with 128 averages. Thus, online integration with current single-voxel spectroscopy MRS acquisition protocol is also possible. Nevertheless, it is worth mentioning that the effectiveness of our postprocessing method is based on three important prerequisites: First, the absolute quantification using internal water as reference requires knowledge of the partial volume fractions of the gray matter, white matter, and cerebrospinal fluid for the voxel acquired as different tissues have different water concentrations and relaxation times (13). Second, for the metabolites with relatively complex spectral lines such as myoinositol and glutamate, the gradient oscillation artifacts need to be removed beforehand to improve the quantification results (9,10,21). Finally, the frame-to-frame variations of the exact voxel locations are better recorded during the sequential MRS scans to alleviate spectral contamination by signals from different regions. Too large a motion, certainly, may cause the scan to be aborted. Theoretically, recording of voxel locations could be potentially achieved with external head position monitoring devices such as MR compatible camera. All the above adjustments should ideally be incorporated in the entire acquisition and processing procedure in order for our algorithm to maximize its usefulness. In this proof-of-principle study, the first and third prerequisites were fulfilled by acquiring NWS spectra from healthy brain tissues predominantly containing white matter only. Even with subject motion (restricted to around 1 cm in this study), the volume fraction of gray matter and cerebrospinal fluid was expected to be less than around 10%, if any. For the second prerequisite, we restricted our in vivo spectral quantification to the region between 1.8 and 3.3 ppm only, such that the influence of gradient oscillation artifacts remains minimal. Results from Fig. 7 show that the artifactual sidebands can be removed by postprocessing, making use of their antiphase symmetry (10,21). In other words, the major conclusions drawn from our study should remain valid.

In our implementation, the unsuppressed water signals are fitted and then separated from the metabolite signals (9,11) using the time-domain MPM method (18). The simulation results from Fig. 4 indicate that better correction is

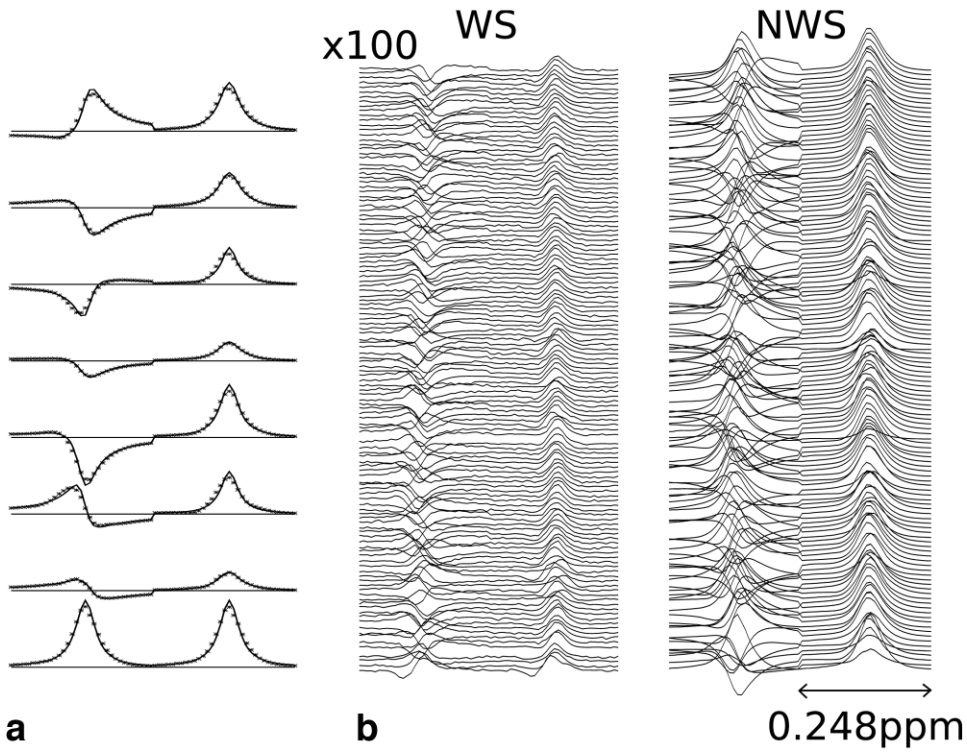

FIG. 6. **a:** Eight consecutive in vivo spectra selected from NWS motion scan with the original water signal (stars) superimposed by the estimated water signal extracted by MPM for the purpose of phase and frequency corrections (solid lines). In each column, spectra of the water signal before and after phase/frequency corrections are shown in the left and right, respectively. **b:** Shot-by-shot spectra acquired from 128 WS motion scans and 128 NWS motion scans. It is seen that phase and frequency corrections using MPM were largely successful even in the presence of various degrees of line-shape asymmetry and broadening.

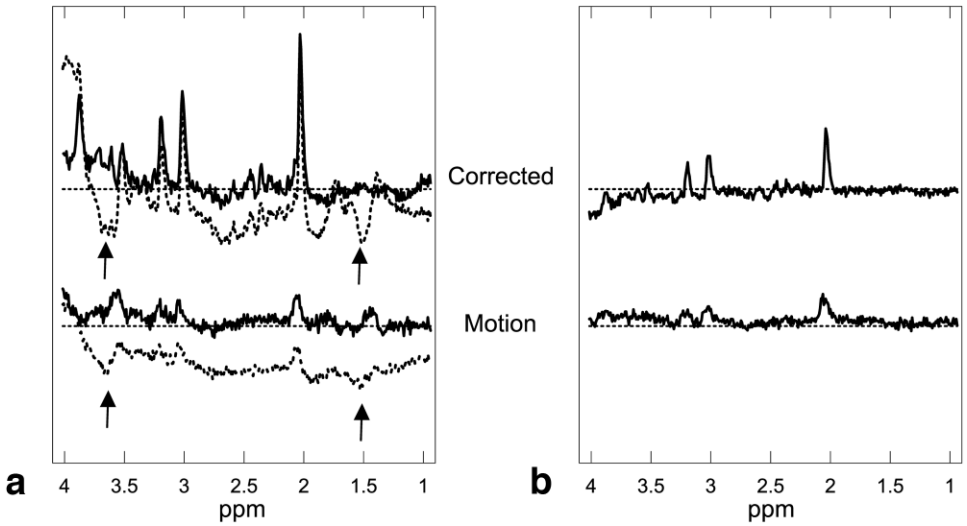

FIG. 7. Spectra obtained in the presence of motion from NWS **(a)** and WS **(b)** acquisitions before (bottom) and after (top) time-domain motion corrections. The sideband artifacts due to gradient oscillations (arrows) as seen on the NWS spectra (dotted line in **(a)**) were removed with additional postprocessing, making use of their symmetric property (solid line in **(a)**). Note that the metabolites quantified in this study are not seriously overlapped with these sidebands located at 1.4 ~ 1.8 ppm and 3.5 ~ 3.8 ppm. The spectra before phase/frequency corrections show severely broadened line width and hence lowered amplitude. The WS spectrum exhibits even worse spectral quality, likely due to distortions from subject movement that results in inconsistent water suppression. The NWS spectrum after time-domain correction has narrower line width (full width at half maximum ~ 10 Hz) compared with the corrected WS spectrum (full width at half maximum ~ 15 Hz).

achieved with higher amplitude of the reference water signal. When the reference water signal is 1000 times larger than NAA, however, the time-domain methods did not show further improvements in phase correction with increasing amplitude of the water signal (Fig. 4). Note that for this part of simulation, only the water signal amplitude was varied, with the metabolite signals and noise amplitude held constant. Thus, the changes of reference signal amplitude essentially paralleled the variations of water signal SNR. The relative independence of motion correction performance on SNR suggests the robustness of the NWS MRS acquisition approach, in that a slight variation in the water content (such as from partial volume averaging with different tissues) plays only a minor role, particularly when using the time-domain MPM algorithm. As a final note, the residual phase errors reported in Fig. 4 did not increase with frequency errors as long as the reference signal amplitude was sufficiently high, which demonstrates the robust performance of the time-domain MPM used in NWS MRS.

We conclude that the NWS MRS with time-domain frame-to-frame corrections is a reliable tool to improve the accuracy of metabolic quantification of in vivo MR spectra in the presence of motion. With the benefits documented in this study, the NWS MRS could be clinically useful for subjects who have difficulties holding still during the MRS scans, such as pediatric patients or those with Parkinson's disease. Other potential applications include the abdominal and thoracic regions, such as breast and liver (23-25), where NWS MRS with frame-to-frame motion corrections may achieve improved performance in the presence of respiratory motion.

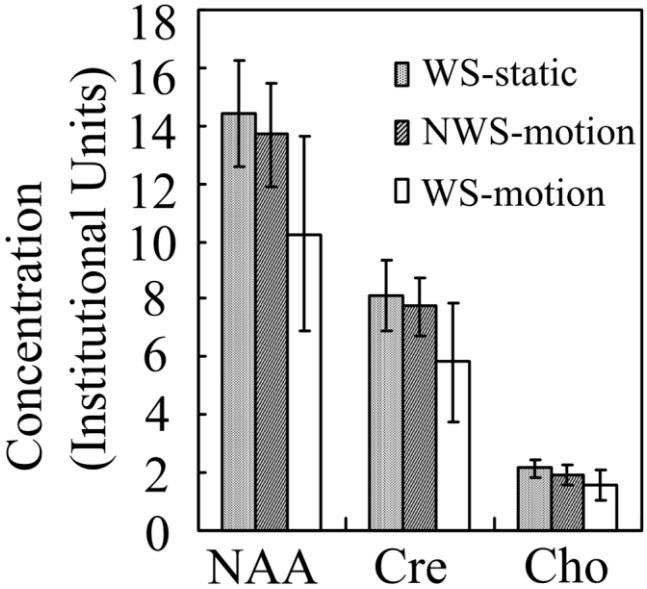

FIG. 8. Concentrations of NAA, tCr, and Cho quantified using time-domain MPM analysis on spectral data obtained from WS-static (shaded), NWS-motion (slashed), and WS-motion (white) scans. The values shown are means and standard deviations from seven subjects. Even after corrections, metabolite concentrations from WS-motion data are significantly lower than those from WS-static scans statistically ($P < 0.02$). The corrected NWS-motion data show better preservation of metabolite concentrations that are insignificantly different ($P > 0.5$) from WS-static results.

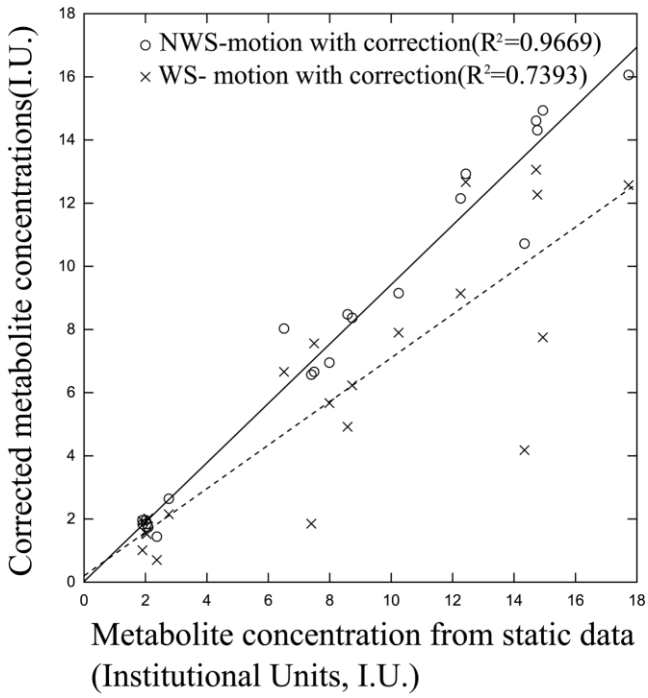

FIG. 9. Correlation of the metabolite concentrations, with the WS-static data treated as true answers for NWS-motion (circles) and WS-motion (crosses) spectra after time-domain motion corrections. The solid and dashed lines are the linear regression lines for NWS-motion and WS-motion results, respectively. The data points are from the three metabolites (NAA, tCr, and Cho) of seven subjects included in this study. NWS-motion exhibits substantially improved correlation with WS-static by showing a regression slope of 0.94, as compared with 0.68 for the WS-motion data.

ACKNOWLEDGMENTS

We thank the National Taiwan University Hospital for permission to use the 3T facilities. J.-M.L. and H.-W.C. were supported in part by the National Science Council under grants NSC 95-2752-B-010-007 and NSC96-2628-E-002-006-MY3, plus grants from the National Health Research Institute. S.-Y.T. received support from the Ministry of Education under the Aim for Top University Project. N.-K.C. received support from the National Parkinson Foundation.

REFERENCES

1. Gabr RE, Sathyanarayana S, Schar M, Weiss RG, Bottomley PA. On restoring motion-induced signal loss in single-voxel magnetic resonance spectra. Magn Reson Med 2006;56:754–760.
2. Thiel T, Czisch M, Elbel GK, Hennig J. Phase coherent averaging in magnetic resonance spectroscopy using interleaved navigator scans: compensation of motion artifacts and magnetic field instabilities. Magn Reson Med 2002;47:1077–1082.
3. Felblinger J, Kreis R, Boesch C. Effects of physiologic motion of the human brain upon quantitative ^{1}H-MRS: analysis and correction by retro-gating. NMR Biomed 1998;11:107–114.
4. Helms G, Piringer A. Restoration of motion-related signal loss and line-shape deterioration of proton MR spectra using the residual water as intrinsic reference. Magn Reson Med 2001;46:395–400.
5. Star-Lack JM, Adalsteinsson E, Gold GE, Ikeda DM, Spielman DM. Motion correction and lipid suppression for ^{1}H magnetic resonance spectroscopy. Magn Reson Med 2000;43:325–330.

6. Posse S, Guenod C, LeBihan D. Motion artifact compensation in ^{1}H spectroscopic imaging by signal tracking. J Magn Reson 1993;102:222–227.
7. Zhu G, Gheorghiu D, Allen PS. Motional degradation of metabolite signal strengths when using STEAM: a correction method. NMR Biomed 1992;5:209–211.
8. Pattany PM, Massand MG, Bowen BC, Quencer RM. Quantitative analysis of the effects of physiologic brain motion on point-resolved spectroscopy. AJNR Am J Neuroradiol 2006;27:1070–1073.
9. Dong Z, Dreher W, Leibfritz D. Toward quantitative short-echo-time in vivo proton MR spectroscopy without water suppression. Magn Reson Med 2006;55:1441–1446.
10. Serrai H, Clayton DB, Senhadji L, Zuo C, Lenkinski RE. Localized proton spectroscopy without water suppression: removal of gradient induced frequency modulations by modulus signal selection. J Magn Reson 2002;154:53–59.
11. Clayton DB, Elliott MA, Leigh JS, Lenkinski RE. 1H spectroscopy without solvent suppression: characterization of signal modulations at short echo times. J Magn Reson 2001;153:203–209.
12. van Der Veen JW, Weinberger DR, Tedeschi G, Frank JA, Duyn JH. Proton MR spectroscopic imaging without water suppression. Radiology 2000;217:296–300.
13. Gasparovic C, Song T, Devier D, Bockholt HJ, Caprihan A, Mullins PG, Posse S, Jung RE, Morrison LA. Use of tissue water as a concentration reference for proton spectroscopic imaging. Magn Reson Med 2006;55:1219–1226.
14. Pels P, Ozturk-Isik E, Swanson MG, Vanhamme L, Kurhanewicz J, Nelson SJ, Van Huffel S. Quantification of prostate MRSI data by model-based time domain fitting and frequency domain analysis. NMR Biomed 2006;19:188–197.
15. van den Boogaart A, Ala-Korpela M, Jokisaari J, Griffiths JR. Time and frequency domain analysis of NMR data compared: an application to 1D ^{1}H spectra of lipoproteins. Magn Reson Med 1994;31:347–358.
16. Vanhamme L, Sundin T, Hecke PV, Huffel SV. MR spectroscopy quantitation: a review of time-domain methods. NMR Biomed 2001;14:233–246.
17. Ratiney H, Coenradie Y, Cavassila S, van Ormondt D, Graveron-Demilly D. Time-domain quantitation of ^{1}H short echo-time signals: background accommodation. Magma 2004;16:284–296.
18. Lin YY, Hodgkinson P, Ernst M, Pines A. A novel detection-estimation scheme for noisy NMR signals: applications to delayed acquisition data. J Magn Reson 1997;128:30–41.
19. Brown MA. Time-domain combination of MR spectroscopy data acquired using phased-array coils. Magn Reson Med 2004;52:1207–1213.
20. Barker PB, Soher BJ, Blackband SJ, Chatham JC, Mathews VP, Bryan RN. Quantitation of proton NMR spectra of the human brain using tissue water as an internal concentration reference. NMR Biomed 1993;6:89–94.
21. Dong Z, Dreher W, Leibfritz D. Experimental method to eliminate frequency modulation sidebands in localized in vivo ^{1}H MR spectra acquired without water suppression. Magn Reson Med 2004;51:602–606.
22. Doyle VL, Buil M, Payne GS, Leach MO. Calculation of sensitivity correction factors for surface coil MRS. Magn Reson Med 1995;33:108–112.
23. Katz-Brull R, Rofsky NM, Lenkinski RE. Breathhold abdominal and thoracic proton MR spectroscopy at 3T. Magn Reson Med 2003;50:461–467.
24. Tyszka JM, Silverman JM. Navigated single-voxel proton spectroscopy of the human liver. Magn Reson Med 1998;39:1–5.
25. Bolan PJ, Henry PG, Baker EH, Meisamy S, Garwood M. Measurement and correction of respiration-induced B0 variations in breast ^{1}H MRS at 4 tesla. Magn Reson Med 2004;52:1239–1245.